Ab Initio Crystal Structure Determination of $VO(H_2PO_2)_2 \cdot H_2O$ from X-ray and Neutron Powder Diffraction Data. A Monodimensional Vanadium(IV) Hypophosphite

A. Le Bail,† M. D. Marcos,‡ and P. Amorós*,‡

Laboratoire des Fluorures, URA CNRS 449, Faculté des Sciences, Université du Maine, 72017 Le Mans, France, and UIBCM, Departament de Química Inorgánica, Facultat de Ciencies Químiques de la Universitat de Valencia, Dr. Moliner 50, 46100-Burjassot, Valencia, Spain

Received November 24, 1993®

The oxovanadium(IV) bis(hypophosphite) hydrate structure is determined *ab initio* from X-ray and neutron powder diffraction data and refined by using the Rietveld method. Samples may present quite different cell parameters, according to the synthesis conditions, although they are described using the same space group ($C2/c$; $Z = 4$) and basically the same structure. Extreme cell parameters values at 25 °C: $a = 12.046(3)$ Å, $b = 8.147(1)$ Å, $c = 7.548(2)$ Å, $\beta = 121.83(2)°$; $a = 12.262$ (8) Å, $b = 8.069(2)$ Å, $c = 7.702(5)$ Å, $\beta = 123.34(5)°$. The structure consists of VO_6 octahedra linked throught bis(μ-hypophosphite-*O,O'*) bridges, giving rise to isolated chains running along the [$\bar{1}$01] direction. The only connection between chains is due to hydrogen bonding involving the coordinated water molecule and one oxygen atom of the H_2PO_2 group. It is suggested that differences among samples are related to additional uncoordinated water molecules randomly inserted between chains (not located). Thermal, IR spectroscopy, and magnetic studies have been performed. X-ray induced amorphization has been followed by powder diffraction and IR spectroscopy.

Introduction

During the two last decades, considerable work has been devoted to the research of new phosphates and phosphonates exhibiting low-dimensional frameworks (chain and layered materials) for applications as catalysts, as cation exchangers, or as molecular sieves.[1-3] Among these compounds, vanadium phosphates have a particularly rich and complex crystal chemistry owing to the variable oxidation state of vanadium and its ability to adopt different coordinations (octahedron, square pyramid, tetrahedron). Low dimensionality is frequent in this family; its influence on magnetic interactions was recently examined in oxovanadium(IV) phosphates.[4]

The interest in oxovanadium phosphates is due in part to the success of one member of this family, $(VO)_2P_2O_7$, in catalyzing the selective air oxidation of butane and butene to maleic anhydride,[5] and it has resulted in a large number of synthesized and characterized materials. A systematic approach to the crystal chemistry and physical properties of oxovanadium phosphates was presented recently, together with a reactivity scheme.[6]

For specific reasons, low dimensionality is favored in phosphites. The phosphite hydrogen atoms behave as "dead ends" in these compounds since they do not bridge to atoms other than phosphorus. Open cavities or tunnels lined by the phosphite hydrogen atoms are very common in HPO_3 pseudotetrahedron-based materials. Influences of H_2PO_2 pseudotetrahedral hypophosphite groups on dimensionality are even more dramatic. As a recent review suggests,[7] the knowledge on such compounds is scarce and, in particular, the lack of data dealing with simple transition metal hypophosphites is remarkable. A very limited number of crystal structure determinations have been reported (that of $Ni(H_2PO_2)_2.6H_2O$;[8] the crystal structures of β-$Mn(H_2PO_2)_2.H_2O$, $Zn(H_2PO_2)_2.H_2O$, and $Zn(H_2PO_2)_2$ determined by Weakley;[9] and those of $CoCl(H_2PO_2).H_2O$[10] and α-$Mn(H_2PO_2)_2.H_2O$[11]). Their magnetic properties remain practically unexplored. This absence of literature data is due, in part, to the difficulties arising in synthesis from solution chemistry related to the redox and acid–base reactions affecting the $H_2PO_2^-$ species and the hydrolytic processes of the cations. In this sense, a synthetic approach was recently proposed to rationalize the preparative chemistry of transition metal hypophosphites, and from very simple ideas it was possible to make reasonable propositions about the metal coordination polyhedron in the solid.[12]

The first reference to oxovanadium(IV) hypophosphite is a 1907 paper by Mawrow.[13] Later, Baran et al.[14] characterized this compound by IR, electronic, and ESR spectroscopy, TG, DTA, and magnetic susceptibility measurements, and X-ray powder diffraction (JCPDS Card 39-0057). The powder pattern, was said to be complex, and indexing was not attempted. As no single crystal was available, the structure remained unknown. By deductions from the formula and from spectroscopic and magnetic measurements, Baran et al.[14] suggested that the structure was constituted by isolated VO_6 octahedra and two $H_2PO_2^-$ anions acting as bidendate ligands occupying the four equatorial coordination positions around the vanadium atoms (also, two crystallographically nonequivalent water molecules were supposed to be present). In this proposition, the remaining coordination positions corresponded to the short V=O bond of the oxovanadium group and the oxygen atom of the coordinated water molecule. Such a bidentate coordination for the $H_2PO_2^-$ groups has never been observed in the hypophosphite family, and we show here

†Université du Maine.
‡Universitat de Valencia.
® Abstract published in *Advance ACS Abstracts,* April 15, 1994.

(1) Kanazawa, T. In *Inorganic Phosphate Materials*; Kanazawe, T., Ed.; Elsevier: Tokyo, 1989.
(2) Clearfield, A. *Chem. Rev.* **1988**, *88*, 125.
(3) Cao, G.; Hong, H.; Mallouk, T. E. *Acc. Chem. Res.* **1992**, *25*, 420.
(4) Amorós, P.; Beltrán, A.; Beltrán, D. *J. Alloys Compounds* **1992**, *188*, 123.
(5) Centi, G.; Trifiro, F.; Ebner, J. R.; Franchetti, V. M. *Chem. Rev.* **1988**, *88*, 55.
(6) Beltrán, D.; Beltrán, A.; Amorós, P.; Ibáñez, R.; Martiñez, E.; Le Bail, A.; Férey, G.; Villeneuve, G. *Eur. J. Solid State Inorg. Chem.* **1991**, *28*, 131.
(7) Loub, J.; Kratochvil, B. *Chem. Listy* **1987**, *81*, 337.
(8) Victor Chemical Works. *Chem. Weekbl.* **1953**, *10*, 40.
(9) Weakley, T. J. R. *Acta Crystallogr., B* **1979**, *25*, 42.
(10) Marcos, M. D.; Ibáñez, R.; Amorós, P.; Le Bail, A. *Acta Crystallogr., C* **1991**, *47*, 1152.
(11) Marcos M. D.; Amorós, P.; Sapiña, F.; Beltrán, D. *J. Alloys Compounds* **1992**, *188*, 133.
(12) Marcos, M. D.; Amorós, P.; Beltrán, A.; Beltrán, D. *Solid State Ionics* **1993**, *63/65*, 96.
(13) Mawrow, F. *Z. Anorg. Allg. Chem.* **1907**, *55*, 147.
(14) Baran, E. J.; Etchevarry, S. B.; Diemann, E. *Polyhedron* **1985**, *4*, 1711.

0020-1669/94/1333-2607$04.50/0

that these groups in $VO(H_2PO_2).H_2O$ act as bis(μ-*O,O'*) bridges leading to a monodimensional structure.

The difficulty in obtaining single crystals of this solid led us to attempt the structure determination from polycrystalline samples. Recent advances in powder diffraction data analysis have made possible the solution of moderately complex structures on the basis of powder diffraction data from either conventional or synchrotron X-rays, more rarely from neutron.[15] We report here the *ab initio* structure determination of the title compound from conventional X-ray and neutron powder diffraction data by using the direct methods. Structure refinements were performed by using the Rietveld method.[16]

Experimental Section

Sample Preparation and Characterization. The synthesis of $VO(H_2PO_2)_2.H_2O$ was carried out as described by Mawrow[13] and Baran et al.[14] by direct reaction between V_2O_5 and hypophosphorous acid. A 1.5-g sample of V_2O_5 (16.4 mmol) was suspended in 10 cm^3 of water; then 4 cm^3 of a 50% H_3PO_2 (37.9 mmol) solution was added dropwise under continuous stirring. The suspension obtained was heated until complete V_2O_5 dissolution and vanadium(V) reduction. During the reaction, the initial orange suspension changed from a green to finally a blue solution.

Varying the reaction temperature and the crystallization time led to samples having not only different crystallinity, as evidenced by anisotropic X-ray line broadening, but also slightly different cell parameters and water contents. Three samples have been chosen as representative: sample I was obtained directly in the reaction vessel (80 °C) by quick concentration of the reacted blue solution, sample II was isolated by allowing slow concentration of the blue mother solution over several days at room temperature, and sample III was also prepared at room temperature but the precipitation required several weeks. The resulting blue solids were filtered off, washed with water and acetone, and air dried.

The solids were dissolved in dilute H_2SO_4 for chemical analysis. V and P concentrations were determined by atomic absorption spectrometry (Perkin-Elmer Zeeman 5000), and the H content was determined by elemental analysis. The water content was determined thermogravimetrically using a Perkin-Elmer TGA-7 analyzer (quick initial heating, 10 °C/min until 100 °C followed by very slow heating, 0.4 °C/min, until 200 °C). The thermal studies were also carried out with a DSC-7 Perkin-Elmer instrument.

The vanadium, phosphorus, and hydrogen analyses for sample I are in good accordance with the content required for the $VO(H_2PO_2)_2.H_2O$ stoichiometry (Anal. Found: V, 23.9; P, 28.6; H, 2.75. Calcd: V, 23.7; P:, 28.8; H, 2.78). On the contrary, samples II and III present slightly deficient contents of vanadium and phosphorus and a small increase in the hydrogen contents (Anal. Found for sample II: V, 23.3; P, 28.0; H, 2.84. Found for sample III: V, 23.1; P, 27.7; H, 2.90). These small differences in composition are consistent with the variations in water loss during the thermogravimetric study of the three samples. It is difficult at this first stage to be sure that the excess of water is not due to adsorbed water. However, both the fact that this small amount of water remains invariable and the observed correlation between the quantity of water and some crystallinity degree suggest the existence of additional water inside the structure. In this sense, a new general formulation would be $VO(H_2PO_2).(1+\delta)H_2O$ and the estimated δ values would be $\delta = 0$ for sample I, $\delta = 0.17$ for sample II, and $\delta = 0.24$ for sample III.

Diffraction Data Collection. X-ray powder diffraction data were collected on a Siemens D501 automated diffractometer. Cu Kα radiation was selected by a graphite monochromator in the reflected beam. Pb$(NO_3)_2$ was used as the internal standard when data for indexation purposes were collected. Although some patterns were recorded up to 130° (2θ), the sensitivity of the samples to X-rays (see below) and a quite large intensity decreasing as a function of the diffracting angle, inclined us to arbitrarily limit data to 73° (2θ) for structure determination and refinement (~150 reflections used). For the selected samples I, II, and III, counting times per step and measurement steps were respectively 14 s, 0.02° (2θ); 28 s, 0.04° (2θ); and 21 s, 0.03° (2θ). In order to minimize the preferred orientation effects, the sample holder described by McMurdie et al. was used.[17]

Neutron powder diffraction data were recorded at room temperature on the D1B instrument at the Institut Laue Langevin (Grenoble) using neutrons of wavelength 2.522 Å. This instrument is equipped with a position-sensitive detector (400 cells) that allows a simultaneous data collection in an angular range of 80° (2θ).[18] Data for sample II were collected in the range 2θ = 15–95° during 30 min (66 reflections used in refinements). All diffraction data were transferred to a VAX computer.

Spectroscopic and Magnetic Measurements. Infrared spectra were recorded on a FT IR Perkin-Elmer 1750 spectrophotometer using dry KBr pellets containing 2% of the sample. The X-band ESR spectrum was recorded on a Bruker ER 200D spectrometer, and magnetic measurements were performed at 0.1 T in the temperature range 2–150 K with a SQUID (SHE) magnetometer–susceptometer.

To test the vanadyl(IV) hypophosphite sensitivity to X-rays, samples were submitted to high irradiation doses from an X-ray fluorescence spectrometer (Siemens SRS200) working at 30 mA and 50 kV and to lower doses from the powder diffractometer (Cu Kα, 28 mA, 38 kV) for a longer time.

Structure Determination and Refinement. Indexing of the X-ray powder pattern of sample I was obtained by using the TREOR program.[19] A probable solution (figures of merit $M_{20} = 23$,[20] $F_{20} = 33$ (0.0089, 68)[21]) was proposed in the monoclinic system; the observed reflection conditions were consistent with the *C*2/*c* and *Cc* space groups. The refined cell parameters were $a = 12.046(3)$ Å, $b = 8.147(1)$ Å, $c = 7.548(2)$ Å, and $\beta = 121.83(2)°$.

Individual $|F_o|$ values were then extracted from the powder pattern by iterating the Rietveld decomposition formula (ARITB program[22]). A large part of the final solution in the *C*2/*c* space group was obtained from the SHELXS-*86* program[23] direct-method facilities: the vanadium, phosphorus, and two oxygen atoms (O(1) and O(2)) were located. Scattering factors and anomalous dispersion corrections were obtained from ref 24. The remaining two oxygen atoms were located from a Fourier difference synthesis performed after a Rietveld refinement (with the ARIT1 program[25]) of the partial structural model. The hydrogen atoms were located from a Fourier difference synthesis following the Rietveld refinement of the neutron powder pattern of sample II (the profile reliabilities R_P[16] with and without hydrogen atoms were respectively 8.0% and 27.1%). In fact, we realized at this stage that samples I and II presented significantly different cell parameters. Moreover, the crystallinities of the two samples were clearly not of the same order, as evidenced by difficulties encountered during the further Rietveld refinement of the X-ray powder diffraction data of sample II (there was no such problem with the neutron data because of the lower instrumental resolution). The problem originated from some reflections which were clearly broader than all the others. The intense (for X-rays) $40\bar{2}$ and $51\bar{3}$ reflections were found particularly broad, and the line broadening was even more dramatic for sample III. In our opinion, this effect is not associated with an anisotropic size effect but more probably with faulting or inhomogeneities (leading to some cell parameters distribution). Additional water could be more or less randomly accommodated between chains, causing some cell distortion responsible for the line broadening. All attempts to locate additional water during refinements of X-ray powder data from samples II and III, or even of the neutron data from sample II, failed. The small quantity to be found corresponds to nearly one-eighth occupancy of a site in a general position and thus is very difficult to detect. Moreover, the sample III X-ray powder pattern is quite difficult to reproduce by using the Rietveld method. An artifice was utilized in order to deal with the line broadening: two sets of reflections were given the possibility of presenting different line widths during the refinement

(15) Cheetham, A. K. In *The Rietveld Method*; Young, R. A., Ed.; Oxford University Press: Oxford, U.K., 1993; p 276.
(16) Rietveld, H. M. *J. Appl. Crystallogr.* **1969**, *2*, 65.
(17) McMurdie, H. F.; Morris, M. C.; Evans, E. H.; Paretzin; B.; Wong, W.; Hubbard, C. R. *Powder Diffr.* **1986**, *1*, 40.
(18) *Guide to Neutron Research Facilities at the ILL*; Blank, H., Maier, B. Eds.; Institut Max von Laue Paul Langevin: Grenoble, France, 1988.
(19) Werner, P.-E.; Eriksson, L.; Westdahl, M. *J. Appl. Crystallogr.* **1985**, *18*, 367.
(20) De Wolff, P. M. *J. Appl. Crystallogr.* **1968**, *1*, 108.
(21) Smith, G. S.; Snyder, R. L. *J. Appl. Crystallogr.* **1979**, *12*, 60.
(22) Le Bail, A. *NIST Spec. Publ.* **1992**, *846*, 213.
(23) Sheldrick, G. M. In *Crystallographic Computing 3*; Sheldrick, G. M., Krüger, C., Goddard, R., Eds.; Clarendon Press: Oxford, U.K., 1985; p 184.
(24) *International Tables for X-Ray Crystallography*; Kynoch: Birmingham, U.K., 1974; Vol. IV.
(25) Le Bail, A. *ARIT1 Program Users Guide*; Université du Maine: Le Mans, France, 1988.

Table 1. Cell Parameters and Discrepancy Factors of Rietveld Refinements for Samples I–III (n for Neutrons)

	cell parameters					*R* factors (%)		
	a (Å)	*b* (Å)	*c* (Å)	*β* (deg)	*V* (Å³)	R_I	R_P	R_{WP}
I	12.046(3)	8.147(1)	7.548(2)	121.83(2)	629.3(5)	3.2	7.0	8.8
II	12.179(4)	8.096(1)	7.638(3)	122.75(3)	633.4(7)	5.2	9.5	11.4
II_n	12.195(5)	8.111(1)	7.651(3)	122.69(3)	636.9(7)	4.6	7.9	5.2
III	12.262(8)	8.069(2)	7.702(5)	123.34(5)	637(1)	8.2	13.4	17.2

Table 2. Atomic Coordinates and Thermal Parameters for $VO(H_2PO_2)_2 \cdot H_2O$ from X-ray Diffraction for Samples I–III and Also from Neutron Diffraction for Sample II_n[a]

atom	sample	*x/a*	*y/b*	*z/c*	*B* (Å²)
V	I	0.0	0.7556(3)	1/4	0.77(5)
	II	0.0	0.7582(4)	1/4	0.37(9)
	II_n	0.0	0.7582	1/4	
	III	0.0	0.7516(6)	1/4	1.6(1)
P	I	0.2271(2)	0.6658(3)	0.7122(4)	1.42(6)
	II	0.2295(3)	0.6646(4)	0.7135(5)	1.4(1)
	II_n	0.227(2)	0.658(2)	0.725(3)	
	III	0.2305(6)	0.6683(6)	0.7057(9)	2.5(2)
O(1)	I	0.1437(3)	0.7861(4)	0.5472(5)	2.15(8)
	II	0.1460(6)	0.7916(7)	0.5456(9)	2.0(1)
	II_n	0.145(1)	0.786(2)	0.553(2)	
	III	0.1549(9)	0.792(1)	0.543(1)	2.8(2)
O(2)	I	0.1274(3)	0.7922(4)	0.1589(5)	2.15(8)
	II	0.1251(6)	0.7910(7)	0.1563(9)	2.0(1)
	II_n	0.122(2)	0.792(2)	0.152(2)	
	III	0.1140(9)	0.786(1)	0.153(1)	2.8(2)
O(3)	I	0.0	1.0337(5)	1/4	2.15(8)
	II	0.0	1.0325(9)	1/4	2.0(1)
	II_n	0.0	1.049(3)	1/4	
	III	0.0	1.015(1)	1/4	2.8(2)
O(4)	I	0.0	0.5653(7)	1/4	2.15(8)
	II	0.0	0.5679(11)	1/4	2.0(1)
	II_n	0.0	0.562(2)	1/4	
	III	0.0	0.567(1)	1/4	2.8(2)
H(1)	II_n	0.181(2)	0.633(2)	0.833(3)	
H(2)	II_n	0.211(2)	0.516(3)	0.624(2)	
H(3)	II_n	0.027(2)	1.121(2)	0.375(3)	

[a] A global $B = 3.5(3)$ Å² thermal parameter was defined for all atoms in the neutron case, and the *y* coordinate of the V atom was fixed to the value obtained from X-ray data.

for all samples (*hkl* with *h* and *l* much greater than *k*, apart from the others). This largely improved the fits, those for sample III remaining however of low quality.

Some details of the final refinements are given in Table 1; the Rietveld discrepancy factors R_P and R_{WP} are the conventional ones[16] (calculated after background subtraction). The final atomic parameters and isotropic *B* factors are gathered in Table 2. The results for sample III and the neutron data for sample II (noted II_n) are the less accurate. Therefore the selected bond lengths and angles are only given for samples I and II in Table 3(however, in the case of sample II, distances and angles are calculated from the X-ray's coordinates with the exception of the hydrogen atom positions originating from the neutron data). Figures 1–4 show the Rietveld fits obtained for samples I, II, II_n, and III, respectively. Tests using the *Cc* space group never improved the results.

Results and Discussion

A preliminary characterization of the three samples using IR spectroscopy (Figure 5) showed that the three spectra were practically identical in both intensities and band energies. However, certain differences among the spectra can be found. In addition to the absorption maxima (3470 and 3520 cm^{-1}) assigned by Baran et al.[14] to the stretching OH modes of the coordinated water molecule, another broad band (3100 cm^{-1}), characteristic of uncoordinated water molecule, is detected. The intensity of this band increases from sample I to samples II and III, the IR spectrum of Baran et al.[14] being similar to that of sample I. An increase in the intensity of the band centered at 590 cm^{-1}, and assignable to the waging H_2O vibrations, is observed from samples I to III.

Table 3. Interatomic Distances (Å) and Angles (deg) of $VO(H_2PO_2)_2 \cdot H_2O$[a]

V octahedron <V-O> = 1.971; 1.966

V	O(4)	O(1)	O(1)	O(2)	O(2)	O(3)
O(4)	**1.550(6)** **1.541(9)**	2.677(4) 2.682(6)	2.677(4) 2.682(6)	2.713(4) 2.697(7)	2.713(4) 2.697(7)	3.816(7) 3.761(11)
O(1)	97.1(4) 97.8(6)	**1.999(2)** **1.997(4)**	3.966(6) 3.958(11)	2.833(5) 2.844(10)	2.780(4) 2.788(9)	2.829(4) 2.778(8)
O(1)	97.1(4) 97.8(6)	165.7(4) 164.4(6)	**1.999(2)** **1.997(4)**	2.780(4) 2.788(9)	2.833(5) 2.844(10)	2.829(4) 2.778(8)
O(2)	98.5(4) 97.6(6)	90.0(3) 90.1(5)	87.9(2) 87.9(5)	**2.007(4)** **2.021(8)**	3.970(3) 4.007(6)	2.795(4) 2.799(7)
O(2)	98.5(4) 97.6(6)	87.9(2) 87.9(5)	90.0(3) 90.1(5)	162.9(2) 164.9(3)	**2.007(4)** **2.021(8)**	2.795(4) 2.799(7)
O(3)	180.0 180.0	82.9(3) 82.2(5)	82.9(3) 82.2(5)	81.5(3) 82.4(5)	81.5(3) 82.4(5)	**2.266(4)** **2.221(7)**

P tetrahedron <P-O> = 1.507; 1.529

P	H(1)	H(2)	O(1)	O(2)
H(1)	**1.35(3)**	2.05(2)	2.37(2)	2.40(3)
H(2)	99(2)	**1.34(2)**	2.33(2)	2.37(2)
O(1)	111(1)	109(2)	**1.484(4)** **1.525(7)**	2.543(3) 2.556(6)
O(2)	112(1)	111(1)	115.3(3) 113.5(5)	**1.529(3)** **1.533(6)**

Water molecule (sample II)

O(3)	H(3)	H(3)
H(3)	**1.09(3)**	1.65(3)
H(3)	98(3)	**1.09(3)**

Hydrogen bonding (sample II)

H(3)...O(2)	1.94(3)	O(3)-O(2)	2.98(4)	O(3)-H(3)-O(2)	157(1)

[a] The first value corresponds to sample I and the second to sample II (using coordinates from X-ray data except those for the hydrogen atoms, which were taken from the neutron data for sample II).

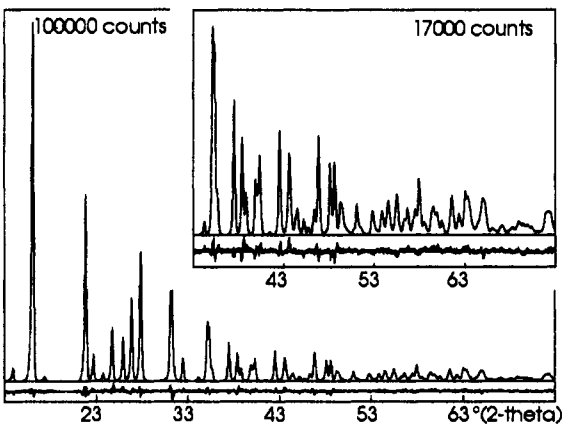

Figure 1. Calculated X-ray diffraction pattern of $VO(H_2PO_2)_2 \cdot H_2O$ (sample I). The observed–calculated difference pattern is below at the same scale.

Thermal Study. In order to clarify the nature of the differences found among the samples, a study of their thermal behavior was carried out. TGA results for sample I are in good accordance with those previously reported by Baran et al.[14]. The first event corresponds basically to the water loss; however, the precise determination of the hydration degree is not straightforward since a partial decomposition of the anion occurs simultaneously. Figure 6 shows the thermal evolution (TGA) of the three samples. In each sample the process begins at a different temperature and is associated with a different weight loss. Though it is difficult to analyze quantitatively this first process, the IR results incline us to assign the differences in weight loss to differences in water content. If sample I has the stoichiometric formulation VO-

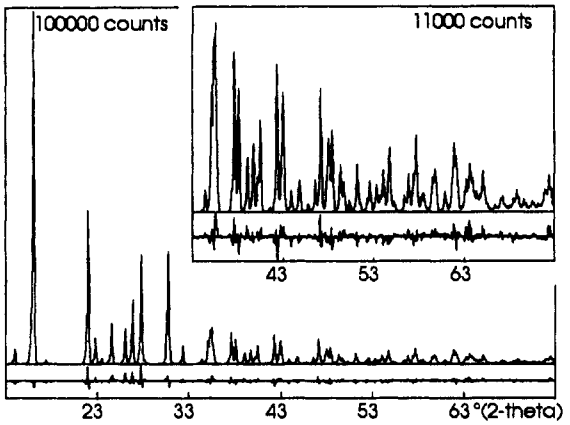

Figure 2. Calculated X-ray diffraction pattern of $VO(H_2PO_2)_2{\cdot}H_2O$ (sample II). The observed–calculated difference pattern is below at the same scale.

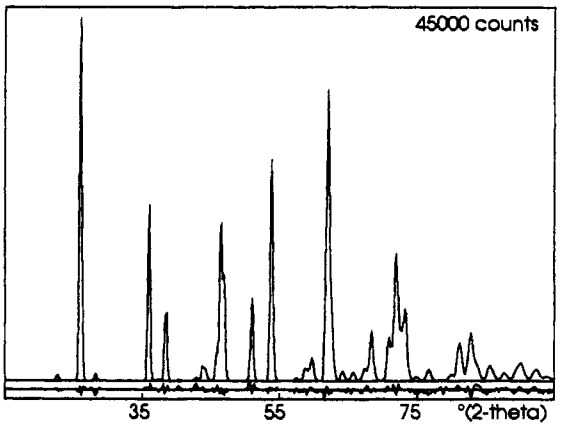

Figure 3. Calculated neutron diffraction pattern of $VO(H_2PO_2)_2{\cdot}H_2O$ (sample II_n). The observed–calculated difference pattern is below at the same scale.

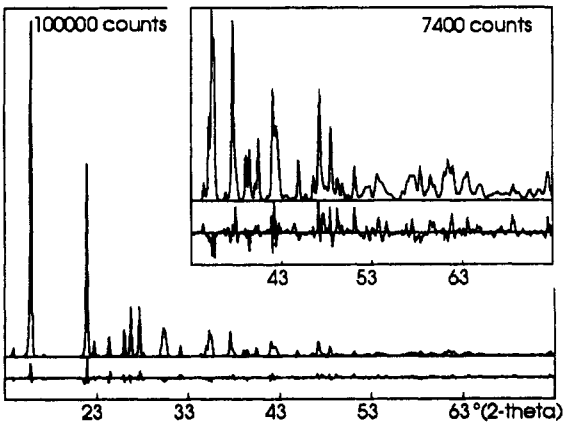

Figure 4. Calculated X-ray diffraction pattern of $VO(H_2PO_2)_2{\cdot}H_2O$ (sample III). The observed–calculated difference pattern is below at the same scale.

$(H_2PO_2)_2.H_2O$, then the estimated additional water content would be $\delta = 0.17$ and $\delta = 0.24$ for samples II and III, respectively (according to the elemental analysis data). The differential scanning calorimetry experiments (Figure 7) could also support the hypothesis of the presence of additional uncoordinated water molecules in samples II and III. The temperature at which the process begins decreases gradually from samples I to III, and also the complexity of this process increases from sample I to III.

Powder Patterns. Differences between samples are evident from their cell parameters (Table 1) or their X-ray powder patterns for $2\theta > 43°$ (note that the cell parameter differences between II and II_n are due to imprecision on the neutron wavelength). The cell parameter evolution is systematic from sample I to sample III. Using 17 of the 20 reflections which can now be unambiguously indexed from the powder data of Baran et al.,[14] one obtains $a = 12.07(1)$ Å, $b = 8.12(1)$ Å, $c = 7.56(1)$ Å, $\beta = 121.89(4)°$, and $V = 629(2)$ Å^3, very near the values characteristic of sample

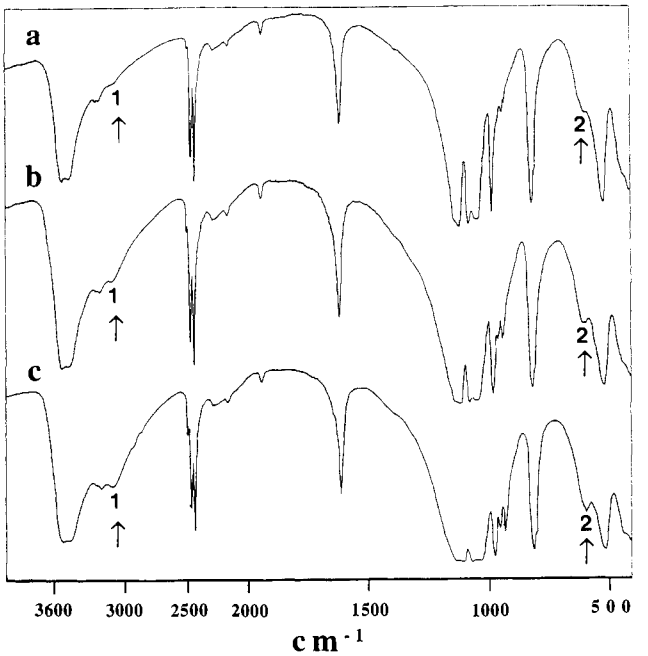

Figure 5. IR spectra of $VO(H_2PO_2)_2{\cdot}H_2O$: (a) sample I; (b) sample II; (c) sample III. The principal differences among the spectra correspond to the marked bands. Bands 1 and 2 correspond to ν(O–H) and $(H_2O)_{wag}$ vibration modes, respectively.

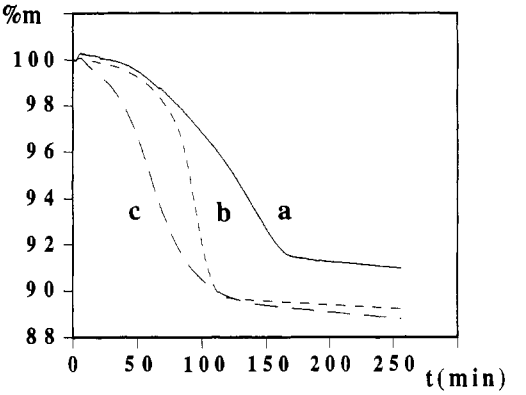

Figure 6. TGA curves of $VO(H_2PO_2)_2{\cdot}H_2O$: (a) sample I; (b) sample II; (c) sample III.

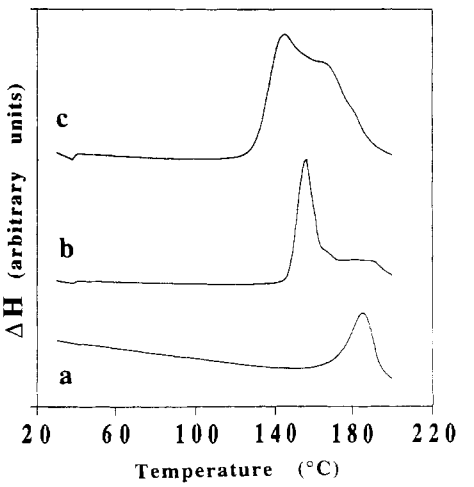

Figure 7. DSC curves of $VO(H_2PO_2)_2{\cdot}H_2O$: (a) sample I; (b) sample II; (c) sample III.

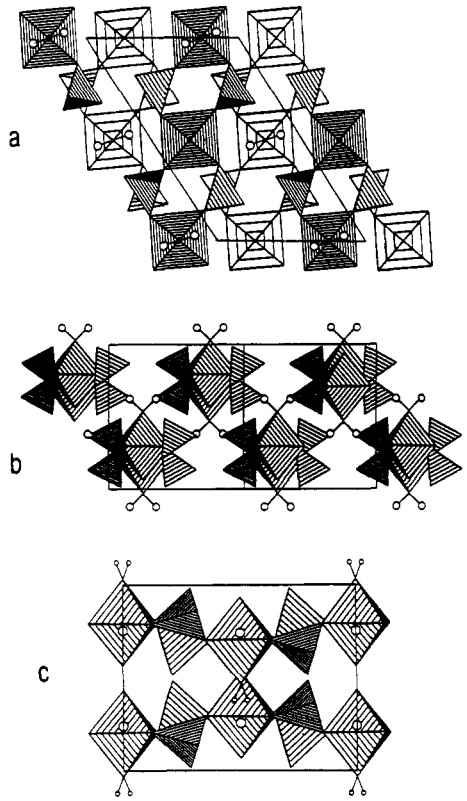

Figure 8. Projection of the structure of $VO(H_2PO_2)_2 \cdot H_2O$: along the (a) [010], (b) [$\bar{1}$01], and (c) [101] directions. VO_6 octahedra are differently dashed in (a) corresponding to chains stacked at different *b* levels. The small circles represent the water hydrogen atoms. The larger ones in (c) correspond to vanadium atoms.

I. Nevertheless, the cell volume does not change so much in the series and this would be an argument for the excess water to be adsorbed, because we cannot locate any void in the structure for its accommodation. Moreover, the atomic coordinates remain quasi-unchanged from samples I to III. However, it must not be forgotten that the structure obtained is a mean one and that we have not access to the structure of faults which are clearly present in these compounds with the effect of broaden some classes of reflections. The view that the hypothetically uncoordinated additional water molecules could be associated with faults, whatever they are, could reconcile the elemental analysis/TGA/IR and powder diffraction results. The low dimensionality leading to some flexibility of the structure may be the reason that the cell distortion seems to be correlated with some degree of faulting, itself associated with the degree of additional water. Finally, the consideration that the various samples could be obtained one from another by thermal treatment was ruled out: a thermodiffraction study of sample II between 150 and 350 K, showed a linear cell parameter variation, characteristic of a simple thermal expansion process.

Description of the Structure. Projections of the structure of sample II along the [010], [$\bar{1}$01] and [101] directions are shown in Figure 8. The model is only slightly modified for the other samples. The structure of $VO(H_2PO_2)_2.H_2O$ consists of linear chains that extend along the [$\bar{1}$01] direction. They are built up from VO_6 octahedra linked through pairs of $H_2PO_2^-$ pseudotetrahedral units acting as bis(μ-*O*,*O*′) bridges. The hydrogen atoms of the water molecule, part of the VO_6 octahedra, are responsible for the interchain cohesion through hydrogen bonding.

The coordination octahedron formed by the oxygen atoms around the vanadium in $VO(H_2PO_2)_2.H_2O$ shows the characteristic anisotropic bonding scheme observed in other oxovanadium(IV) derivatives.[6] The four equatorial oxygen atoms are shared with four different $H_2PO_2^-$ groups. The two apical V–O bonds are perpendicular to the propagation chain direction. One

Table 4. Valence-Bond analysis for $VO(H_2PO_2)_2 \cdot H_2O$ (Sample I) Using the Zachariasen Law[a]

	V	P	Σ
O(1)	0.56 ×2	1.38	1.94
O(2)	0.55 ×2	1.23	1.78
O(3)	0.27		0.27
O(4)	1.88		1.88
Σ	4.37	2.61	

[a] $s = \exp[-(R - R_0)/B]$; $R_0 = 1.784$ and $B = 0.37$ for V and 1.604 and 0.37 for P.[27]

corresponds to the oxovanadium group and its length is the shortest, indicating multiple-bond character. One must note that the accuracy of this study from powder data is by no way comparable to the accuracy expected from a single-crystal study. The V=O distance is probably too short here by 0.05 Å since usually it is near of 1.60 Å. In *trans*-position to this double bond is the coordinated water molecule. In each chain the VO_6 octahedra are alternatively disposed at different *b* levels and show a cooperative twisting of the equatorial planes around the V=O bond, giving rise to a nonfaced disposition of the O(1)–O(2) octahedral edges. Along these slightly corrugated chains, the V=O bonds alternately point up and down relative to the *ac* plane.

As was proposed by Baran et al.,[14] on the basis of IR spectroscopic data, the $H_2PO_2^-$ entities adopt a symmetry lower than C_{2v}; however, their suggestion that the $H_2PO_2^-$ pseudotetrahedral units share a common O–O edge with the VO_6 octahedra is wrong, they share corners with two different octahedra. The two $H_2PO_2^-$ groups of each bis(μ-*O*,*O*′) bridge are related by an inversion center, and the respective P–H bonds are alternately directed up and down in relation to the *ac* plane. The bond distances and angles in the distorted $H_2PO_2^-$ tetrahedra are similar to those observed in other hypophosphite compounds.[9-11] The P–O(2) bond is slightly longer than the P–O(1) one for both samples I and II. This could be related to involvement of the O(2) atoms in the interchain hydrogen-bonding network at variance to O(1). The two independent P–H bonds present almost identical short distances, as usual (sample II), and the corresponding H atoms are not concerned with any other interaction.

The role of the $H_2PO_2^-$ bridges may be determinant in establishing the true structural dimensionality of the considered materials. In fact, as indicated above, although the initial approach in our investigation of hypophosphite derivatives was to favor the lowering of the structural dimensionality by going from PO_4^{3-} to $H_2PO_2^-$, the result in practice is that a given anion, such as $H_2PO_2^-$, can give rise to structures ranging from 1-D, *e.g.* $VO(H_2PO_2)_2.H_2O$, to 3-D, *e.g.* α-$M(H_2PO_2)_2.H_2O$ (M = Zn, Mn).[9,10] In the case of oxovanadium(IV) hypophosphite, both the presence of bis(μ-*O*,*O*′) bridges and the characteristic anisotropy of the VO^{2+} cation cooperate to yield a truly one-dimensional system.

The water molecules coordinated to vanadium atoms show C_{2v} symmetry. The O–H bond length is 1.09 Å, a value slightly larger than that found in other hydrated oxovanadium compounds. This could be explained by the participation of the H(3) atoms in the hydrogen interactions that cross-link the chains at different *b* levels. One chain shows hydrogen bonding with four other chains, two up and two down the *b* axis through the P–O(2)...H-(3)–O(3)–H(3)...O(2)–P scheme. According to the hydrogen-bond classification proposed by Lutz[26] for water molecules, the title compound has a bent-symmetric hydrogen bond of moderate strength that is solely responsible for the interchain cohesion.

A bond valence analysis performed for sample I (Table 4)

(26) Lutz, H. D. *Struct. Bonding* **1988**, *69*, 97.
(27) Brese, N. E.; O'Keeffe, M. *Acta Crystallogr., B* **1991**, *47*, 192.

Table 5. Cell Parameter Variations of $VO(H_2PO_2)_2 \cdot H_2O$ (Sample II) with the X-ray Exposure Time (28 mA, 38 kV, Cu K)[a]

exposure time (days)	a (Å)	b (Å)	c (Å)	β (deg)	V (Å^3)	no. of reflns
0	12.175(1)	8.102(1)	7.632(1)	122.68(1)	633.6	51
16	12.177(1)	8.105(1)	7.634(1)	122.68(1)	634.2	49
19	12.189(1)	8.098(1)	7.637(1)	122.76(1)	633.9	46
22	12.200(1)	8.094(1)	7.642(1)	122.80(1)	634.3	41
25	12.205(2)	8.095(1)	7.644(1)	122.81(1)	634.7	35
39	12.216(2)	8.086(1)	7.649(1)	122.89(1)	634.5	32

[a] The number of reflections retained for refinement is given.

confirms the weak link of O(3) to the vanadium atom and verifies the O(2) participation in hydrogen bonding. The expected valences of respectively 4, 3, and 2 for the V, P, and O(1) and O(4) atoms are verified within 10% error. Due to a lower accuracy, such a valence analysis leads to a larger error for sample II and even a larger one for sample III.

Related Compounds. Using the mineral structural classification proposed by Hawthorne,[28] we could consider $VO(H_2PO_2)_2.H_2O$ as belonging to the group characterized by $[M(TO_4)_2\Phi_2]$ type chains (M = octahedrally coordinated cations with the highest bond valence; T = tetrahedral entities; Φ = other ligands). This type of chain is the basis of the minerals kröhnkite, $Na_2[Cu(SO_4)_2(H_2O)_2]$, talmessite, $Ca_2[Mg(AsO_4)_2(H_2O)_2]$, and fairfieldite $Ca_2[Mn(PO_4)_2(H_2O)_2]$. The three groups differ principally in the hydrogen bonding schemes. The main cohesion between chains in these minerals is provided by the inserted alkaline or alkaline earth cations, contrary to the case of the title compound, for which there is no such inserted cation.

Evolution of $VO(H_2PO_2)_2.H_2O$ Induced by Exposure to X-rays. During X-ray measurement, we noticed a change from blue to greenish in the color of exposed samples. Indeed, very prolonged exposure of sample II to radiation from the conventional X-ray diffractometer led to systematic cell parameter variations, although the cell volume remained practically unchanged (see Table 5). These modifications were accompanied by a progressive degradation of the crystallinity evidenced by an increase in the line broadening.

The effect of much more significant doses from a fluorescence rotatory anode applied to sample III (under vacuum) was also observed. In this case an exposure of 36 h was sufficient to produce an amorphous yellow solid with a flat powder pattern. The color change is indicative of the vanadium(IV) to vanadium(V) oxidation, which should be related to an internal redox reaction. Both ligands in this compound could act as internal oxidizing agents, *i.e.* the water molecule

$$VO(H_2PO_2)_2 \cdot H_2O \rightarrow VO(OH)(H_2PO_2)_2 + {}^1/_2H_2\uparrow$$

and the hypophosphite anion

$$VO(H_2PO_2)_2 \cdot H_2O \rightarrow VO_2(HPO_3)_2 + {}^1/_2PH_3\uparrow$$

The first reaction would give rise to a very few changes in the bond scheme, while the second one would lead the breaking down of the structure. Since the final product is an amorphous solid and also the reaction has a superficial character, the analysis of the resulting solid is very complex. Only an IR study of the sample could help us to propose a possible mechanism. The evolution of the IR spectra of sample III is shown in Figure 9. The principal feature is the broadening of all bands associated to the crystallinity loss. This broadening would even be exaggerated by the formation of other oxoanions such as HPO_3^{2-}, whose absorption bands appear very close to the hypophosphite ones. The intensity decrease of the band associated with the $(PH_2)_{wag}$ vibration (807 cm^{-1}) together with the increase of the band that could be associated with $\nu(PO_3)_{sym}$ (945 cm^{-1}) would

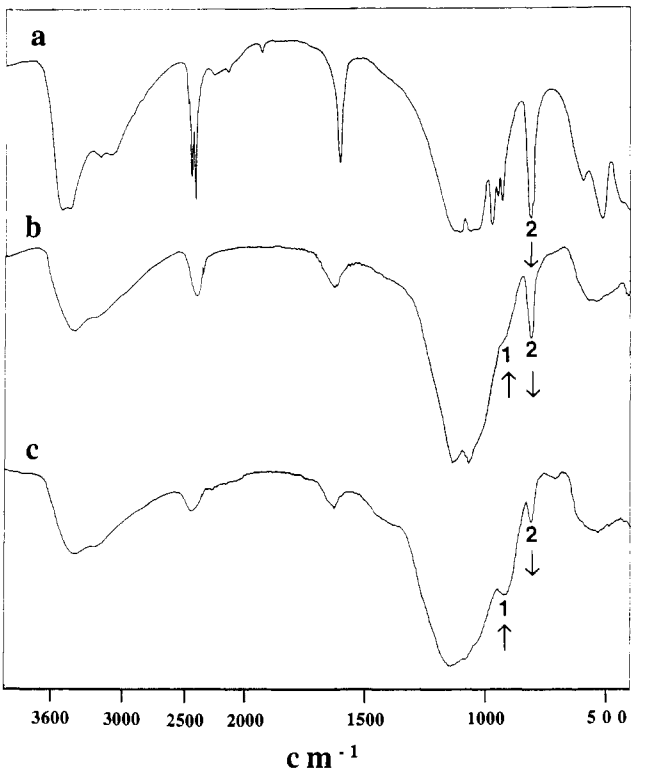

Figure 9. X-radiation-induced evolution of $VO(H_2PO_2)_2 \cdot H_2O$ (sample III) followed by IR spectroscopy. Irradiation times: (a) 0 h; (b) 24 h, (c) 48 h. Bands 1 and 2 can be assigned to the $\nu(PO_3)_{sim}$ vibration mode of HPO_3 groups and $(PH_2)_{wag}$ vibration mode of H_2PO_2 groups, respectively.

support a mechanism based on the second redox reaction. On the other hand, the absence of any band in the high-energy stretching (OH) zone indicates the absence of OH^- groups in the decomposition product.

It would be necessary to perform experiments to identify the decomposition products in order to establish the nature of this process unambiguously way. However, our data are consistent with an internal redox process in which X-radiation induces disproportionation of the hypophosphite anion with a concomitant oxidation of the vanadium(IV) cation. Such disproportionation would give rise to the breaking of some μ-*O,O'* bridges, and this would produce an expansion of the structure mainly in the *ac*, plane allowing us perhaps to explain the cell parameter variations in Table 5.

Magnetic Study. Shown in Figure 10 is the temperature dependence of the reciprocal molar susceptibility of $VO(H_2PO_2)_2.H_2O$ (sample I). Between 2 and 200 K, the data are described very well by a Curie–Weiss behavior: $\chi_m = C/(T-\Theta)$, where $C = 0.376$ cm^3.K.mol^{-1} and $\Theta = -7.81$ K. From the relation $C = N\mu_{eff}^2/3k_B$ one obtains the effective magnetic moment $\mu_{eff} = 1.732\ \mu_B$ per vanadium atom, which is in good agreement with the spin-only value of 1.73 μ_B for a d^1 ion. These values are very similar to those previously reported by Baran et al.[14] from 100–300 K data. Our complementary data show no evidence of long-range or low dimensional magnetic interactions down to 2 K.

The X-band ESR spectrum of $VO(H_2PO_2)_2.H_2O$ (sample I) recorded at room temperature (see Figure 11) shows a practically isotropic signal from which a g value of 1.97 is obtained. Moreover, the ESR spectrum clearly shows a half-field signal generally associated with low-dimensional magnetic systems. Indeed, the $\Delta M_s = 2$ transition is not completely forbidden due to dipolar coupling. Such a signal is frequently observed in dimers ($VO(HPO_4).0.5H_2O$ and α-$VO(HPO_4).2H_2O$),[6,29] but it can also

(28) Hawthorne, F. C. *Am. Mineral.* **1985**, *70*, 455.

(29) Villeneuve, G.; Suh, K. S.; Amorós, P.; Casañ-Pastor, N.; Beltrán, D. *Chem. Mater.* **1992**, *4*, 108.

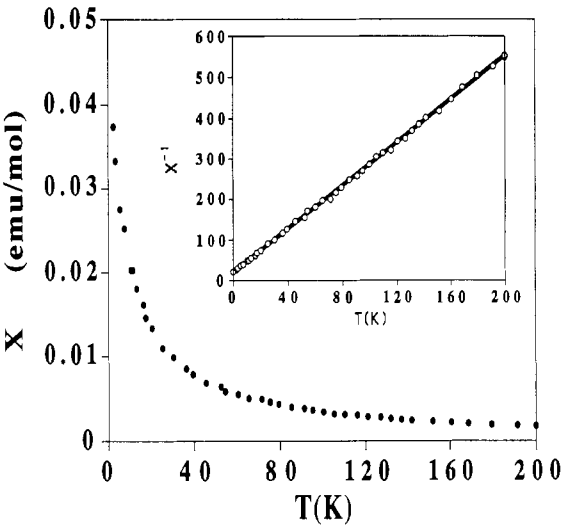

Figure 10. Plot of χ_m *vs* T for $VO(H_2PO_2)_2 \cdot H_2O$ (sample I). In the inset is represented the temperature dependence of the inverse of the molar susceptibility.

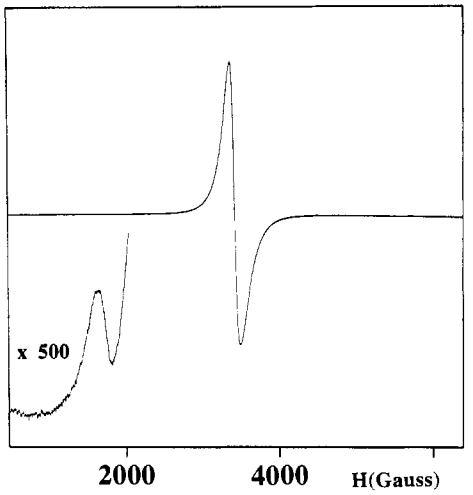

Figure 11. X-Band ESR spectrum of $VO(H_2PO_2)_2 \cdot H_2O$ (sample I) recorded at room temperature. In the inset is shown the $\Delta M_s = \pm 2$ forbidden signal.

be observed in chains such as $N(CH_3)_4MnCl_3$,[30,31] $VO(HPO_4) \cdot 4H_2O$,[6,32] and $(VO)_2P_2O_7$,[6,32] and it would theoretically appear in 2-D magnetic systems. In this context, the observed $\Delta M_s = 2$ signal constitutes the only evidence of low-dimensional magnetic interactions in $VO(H_2PO_2)_2.H_2O$. Its detection suggests that, very likely, some vanadium to vanadium interaction through the bis(μ-hypophosphite-O,O') groups take place.

Magnetic superexchange involving diamagnetic tetrahedral anions such as SO_4^{2-}, PO_4^{3-}, AsO_4^{3-}, MoO_4^{2-}, and ReO_4^- has been reported in the literature.[33] The involvement of phosphate groups in the spin transfer between vanadium atoms in oxovanadium(IV) phosphates ($VO(HPO_4).nH_2O$ (n = 0.5, 1, 2 (α), 2 (β), 4) and $(VO)_2P_2O_7$) has been proved unambiguously by using ^{31}P solid-state NMR as a local probe.[6,29,32] On the basis of topological considerations about the different bridging modes of the phosphate groups in oxovanadium(IV) phosphates, a consistent qualitative interpretation of the observed magnetic properties has been done.[4,6,32]

The bis(μ-hypophosphite-O,O') bridges in the title compound show simultaneously the particularities observed in the corresponding bis(μ-monohydrogen phosphite-O,O') bridges in β-$VO(HPO_4).2H_2O$ (twisted VO_6 octahedra),[34] $VO(HPO_4).4H_2O$ (VO_6 octahedra at different levels),[35] and $VO(HPO_4).0.5H_2O$ (nonfaced VO_6 entities).[35,36] In all three cases, these unfavorable arrangements yield, as probably occurs in the $VO(H_2PO_2)_2.H_2O$ very small magnetic interactions.

It seems reasonable to conclude that the magnetic properties of transition metal hypophosphites will be also highly dependent on the possible involvement of the phosphorus orbitals in the propagation of magnetic interactions. In the case of $VO(H_2PO_2)_2.H_2O$, if we consider the bis(μ-H_2PO_2-O,O') bridges active and take into account their structural features, only a 1-D magnetic behavior could be expected.

More work and experiments, at very low temperature, in the case of $VO(H_2PO_2)_2.H_2O$ are needed in order to establish in a conclusive way the participation of hypophosphite groups in the transmission of the magnetic interaction.

Acknowledgment. M.D.M. thanks the Spanish Ministerio de Educación y Ciencia for a FPI fellowship. M.D.M. and P.A. are very grateful to the Institucio Valenciana d'Estudis i Investigacio (IVEI) and the DGICYT of the Spanish Ministerio de Educación y Ciencia (Grant PB91-0559) for partial financial support of this work. The authors thank the Institut Laue Langevin (Grenoble) for providing neutron facilities.

(30) Dietz, R. E.; Merrit, F. R.; Dingle, R.; Hone, D.; Silbernagel, B. G.; Richards, P. M. *Phys. Rev. Lett.* **1971**, *26*, 1186.
(31) Bencini, A.; Gatteschi, D. *Electron Paramagnetic Resonance of Exchanged Coupled Systems*; Springer Verlag: Berlin, 1990.
(32) Beltrán, D.; Amorós, P.; Ibáñez, R.; Martiñez, E.; Beltrán, A.; Le Bail, A.; Férey, G.; Villeneuve, G. *Solid State Ionics* **1989**, *32/33*, 57.
(33) Charron, F. F.; Reiff, W. M. *J. Solid State Chem.* **1985**, *58*, 38.
(34) Le Bail, A.; Ferey, G.; Amorós, P.; Beltrán, D.; Villeneuve, G. *J. Solid State Chem.* 1989, *79*, 169.
(35) Leonowicz, M. E.; Johnson, J. W.; Brody, J. F.; Shanson; H. F.; Newsam, J. M. *J. Solid State Chem.* **1985**, *56*, 370.
(36) Torardi, C. C.; Calabrese, J. C. *Inorg. Chem.* **1984**, *23*, 1308.